Transverse single-spin asymmetry of charged hadrons at forward and backward rapidity in polarized $p+p$, $p+$Al, and $p+$Au collisions at $\sqrt{s_{NN}} = 200$ GeV

N. J. Abdulameer,[14] U. Acharya,[19] C. Aidala,[40] Y. Akiba,[54,55,*] M. Alfred,[21] V. Andrieux,[40] N. Apadula,[26] H. Asano,[32,54] B. Azmoun,[7] V. Babintsev,[22] N. S. Bandara,[38] K. N. Barish,[8] S. Bathe,[5,55] A. Bazilevsky,[7] M. Beaumier,[8] R. Belmont,[11,47] A. Berdnikov,[57] Y. Berdnikov,[57] L. Bichon,[65] B. Blankenship,[65] D. S. Blau,[31,44] J. S. Bok,[46] V. Borisov,[57] M. L. Brooks,[34] J. Bryslawskyj,[5,8] V. Bumazhnov,[22] S. Campbell,[12] V. Canoa Roman,[60] R. Cervantes,[60] M. Chiu,[7] C. Y. Chi,[12] I. J. Choi,[23] J. B. Choi,[28,†] Z. Citron,[66] M. Connors,[19,55] R. Corliss,[60] Y. Corrales Morales,[34] N. Cronin,[60] M. Csanád,[15] T. Csörgő,[39,67] T. W. Danley,[48] M. S. Daugherity,[1] G. David,[7,60] C. T. Dean,[34] K. DeBlasio,[45] K. Dehmelt,[60] A. Denisov,[22] A. Deshpande,[55,60] E. J. Desmond,[7] A. Dion,[60] D. Dixit,[60] V. Doomra,[60] J. H. Do,[68] A. Drees,[60] K. A. Drees,[6] J. M. Durham,[34] A. Durum,[22] H. En'yo,[54] A. Enokizono,[54,56] R. Esha,[60] B. Fadem,[42] W. Fan,[60] N. Feege,[60] D. E. Fields,[45] M. Finger, Jr.,[9] M. Finger,[9] D. Firak,[14,60] D. Fitzgerald,[40] S. L. Fokin,[31] J. E. Frantz,[48] A. Franz,[7] A. D. Frawley,[18] Y. Fukuda,[64] P. Gallus,[13] C. Gal,[60] P. Garg,[3,60] H. Ge,[60] M. Giles,[60] F. Giordano,[23] Y. Goto,[54,55] N. Grau,[2] S. V. Greene,[65] M. Grosse Perdekamp,[23] T. Gunji,[10] H. Guragain,[19] T. Hachiya,[43,54,55] J. S. Haggerty,[7] K. I. Hahn,[16] H. Hamagaki,[10] H. F. Hamilton,[1] J. Hanks,[60] S. Y. Han,[16,30] M. Harvey,[62] S. Hasegawa,[27] T. O. S. Haseler,[19] T. K. Hemmick,[60] X. He,[19] J. C. Hill,[26] K. Hill,[11] A. Hodges,[19,23] R. S. Hollis,[8] K. Homma,[20] B. Hong,[30] T. Hoshino,[20] N. Hotvedt,[26] J. Huang,[7] K. Imai,[27] M. Inaba,[64] A. Iordanova,[8] D. Isenhower,[1] D. Ivanishchev,[52] B. V. Jacak,[60] M. Jezghani,[19] X. Jiang,[34] Z. Ji,[60] B. M. Johnson[ORCID],[7,19] D. Jouan,[50] D. S. Jumper,[23] J. H. Kang,[68] D. Kapukchyan,[8] S. Karthas,[60] D. Kawall,[38] A. V. Kazantsev,[31] V. Khachatryan,[60] A. Khanzadeev,[52] A. Khatiwada,[34] C. Kim,[8,30] E.-J. Kim,[28] M. Kim,[58] T. Kim,[16] D. Kincses,[15] A. Kingan,[60] E. Kistenev,[7] J. Klatsky,[18] P. Kline,[60] T. Koblesky,[11] D. Kotov,[52,57] L. Kovacs,[15] S. Kudo,[64] B. Kurgyis,[15,60] K. Kurita,[56] Y. Kwon,[68] J. G. Lajoie,[26] D. Larionova,[57] A. Lebedev,[26] S. Lee,[68] S. H. Lee,[26,40,60] M. J. Leitch,[34] Y. H. Leung,[60] N. A. Lewis,[40] S. H. Lim,[34,53,68] M. X. Liu,[34] X. Li,[34] V.-R. Loggins,[23] D. A. Loomis,[40] K. Lovasz,[14] D. Lynch,[7] S. Lökös,[15] T. Majoros,[14] Y. I. Makdisi,[6] M. Makek,[69] V. I. Manko,[31] E. Mannel,[7] M. McCumber,[34] P. L. McGaughey,[34] D. McGlinchey,[11,34] C. McKinney,[23] M. Mendoza,[8] A. C. Mignerey,[37] A. Milov,[66] D. K. Mishra,[4] J. T. Mitchell,[7] M. Mitrankova,[57] Iu. Mitrankov,[57] G. Mitsuka,[29,55] S. Miyasaka,[54,63] S. Mizuno,[54,64] M. M. Mondal,[60] P. Montuenga,[23] T. Moon,[30,68] D. P. Morrison,[7] A. Muhammad,[41] B. Mulilo,[30,54,70] T. Murakami,[32,54] J. Murata,[54,56] K. Nagai,[63] K. Nagashima,[20] T. Nagashima,[56] J. L. Nagle,[11] M. I. Nagy,[15] I. Nakagawa,[54,55] K. Nakano,[54,63] C. Nattrass,[61] S. Nelson,[17] T. Niida,[64] R. Nouicer,[7,55] N. Novitzky,[60,64] T. Novák,[39,67] G. Nukazuka,[54,55] A. S. Nyanin,[31] E. O'Brien,[7] C. A. Ogilvie,[26] J. Oh,[53] J. D. Orjuela Koop,[11] M. Orosz,[14] J. D. Osborn,[7,40,49] A. Oskarsson,[35] G. J. Ottino,[45] K. Ozawa,[29,64] V. Pantuev,[24] V. Papavassiliou,[46] J. S. Park,[58] S. Park,[41,54,58,60] M. Patel,[26] S. F. Pate,[46] W. Peng,[65] D. V. Perepelitsa,[7,11] G. D. N. Perera,[46] D. Yu. Peressounko,[31] C. E. PerezLara,[60] J. Perry,[26] R. Petti,[7] M. Phipps,[7,23] C. Pinkenburg,[7] R. P. Pisani,[7] M. Potekhin,[7] A. Pun,[48] M. L. Purschke,[7] P. V. Radzevich,[57] N. Ramasubramanian,[60] K. F. Read,[49,61] D. Reynolds,[59] V. Riabov,[44,52] Y. Riabov,[52,57] D. Richford,[5] T. Rinn,[23,26] S. D. Rolnick,[8] M. Rosati,[26] Z. Rowan,[5] J. Runchey,[26] A. S. Safonov,[57] T. Sakaguchi,[7] H. Sako,[27] V. Samsonov,[44,52] M. Sarsour,[19] S. Sato,[27] B. Schaefer,[65] B. K. Schmoll,[61] K. Sedgwick,[8] R. Seidl,[54,55] A. Sen,[26,61] R. Seto,[8] A. Sexton,[37] D. Sharma,[60] I. Shein,[22] M. Shibata,[43] T.-A. Shibata,[54,63] K. Shigaki,[20] M. Shimomura,[26,43] T. Shioya,[64] Z. Shi,[34] P. Shukla,[4] A. Sickles,[23] C. L. Silva,[34] D. Silvermyr,[35] B. K. Singh,[3] C. P. Singh,[3] V. Singh,[3] M. Slunečka,[9] K. L. Smith,[18] M. Snowball,[34] R. A. Soltz,[33] W. E. Sondheim,[34] S. P. Sorensen,[61] I. V. Sourikova,[7] P. W. Stankus,[49] S. P. Stoll,[7] T. Sugitate,[20] A. Sukhanov,[7] T. Sumita,[54] J. Sun,[60] Z. Sun,[14] J. Sziklai,[67] R. Takahama,[43] K. Tanida,[27,55,58] M. J. Tannenbaum,[7] S. Tarafdar,[65,66] A. Taranenko,[44,59] G. Tarnai,[14] R. Tieulent,[19,36] A. Timilsina,[26] T. Todoroki,[54,55,64] M. Tomášek,[13] C. L. Towell,[1] R. S. Towell,[1] I. Tserruya,[66] Y. Ueda,[20] B. Ujvari,[14] H. W. van Hecke,[34] J. Velkovska,[65] M. Virius,[13] V. Vrba,[13,25] N. Vukman,[69] X. R. Wang,[46,55] Z. Wang,[5] Y. S. Watanabe,[10] C. P. Wong,[19,34] C. L. Woody,[7] L. Xue,[19] C. Xu,[46] Q. Xu,[65] S. Yalcin,[60] Y. L. Yamaguchi,[60] H. Yamamoto,[64] A. Yanovich,[22] I. Yoon,[58] J. H. Yoo,[30] I. E. Yushmanov,[31] H. Yu,[46,51] W. A. Zajc,[12] A. Zelenski,[6] and L. Zou[8]

(PHENIX Collaboration)

[1]*Abilene Christian University, Abilene, Texas 79699, USA*
[2]*Department of Physics, Augustana University, Sioux Falls, South Dakota 57197, USA*
[3]*Department of Physics, Banaras Hindu University, Varanasi 221005, India*
[4]*Bhabha Atomic Research Centre, Bombay 400 085, India*
[5]*Baruch College, City University of New York, New York, New York, 10010 USA*
[6]*Collider-Accelerator Department, Brookhaven National Laboratory, Upton, New York 11973-5000, USA*

[7]*Physics Department, Brookhaven National Laboratory, Upton, New York 11973-5000, USA*
[8]*University of California-Riverside, Riverside, California 92521, USA*
[9]*Charles University, Faculty of Mathematics and Physics, 180 00 Troja, Prague, Czech Republic*
[10]*Center for Nuclear Study, Graduate School of Science, University of Tokyo,*
7-3-1 Hongo, Bunkyo, Tokyo 113-0033, Japan
[11]*University of Colorado, Boulder, Colorado 80309, USA*
[12]*Columbia University, New York, New York 10027*
and Nevis Laboratories, Irvington, New York 10533, USA
[13]*Czech Technical University, Zikova 4, 166 36 Prague 6, Czech Republic*
[14]*Debrecen University, H-4010 Debrecen, Egyetem tér 1, Hungary*
[15]*ELTE, Eötvös Loránd University, H-1117 Budapest, Pázmány P. s. 1/A, Hungary*
[16]*Ewha Womans University, Seoul 120-750, Korea*
[17]*Florida A&M University, Tallahassee, Florida 32307, USA*
[18]*Florida State University, Tallahassee, Florida 32306, USA*
[19]*Georgia State University, Atlanta, Georgia 30303, USA*
[20]*Physics Program and International Institute for Sustainability with Knotted Chiral Meta Matter*
(SKCM2), Hiroshima University, Higashi-Hiroshima, Hiroshima 739-8526, Japan
[21]*Department of Physics and Astronomy, Howard University, Washington, DC 20059, USA*
[22]*IHEP Protvino, State Research Center of Russian Federation, Institute for High Energy Physics,*
Protvino, 142281, Russia
[23]*University of Illinois at Urbana-Champaign, Urbana, Illinois 61801, USA*
[24]*Institute for Nuclear Research of the Russian Academy of Sciences,*
prospekt 60-letiya Oktyabrya 7a, Moscow 117312, Russia
[25]*Institute of Physics, Academy of Sciences of the Czech Republic,*
Na Slovance 2, 182 21 Prague 8, Czech Republic
[26]*Iowa State University, Ames, Iowa 50011, USA*
[27]*Advanced Science Research Center, Japan Atomic Energy Agency,*
2-4 Shirakata Shirane, Tokai-mura, Naka-gun, Ibaraki-ken 319-1195, Japan
[28]*Jeonbuk National University, Jeonju 54896, Korea*
[29]*KEK, High Energy Accelerator Research Organization, Tsukuba, Ibaraki 305-0801, Japan*
[30]*Korea University, Seoul 02841, Korea*
[31]*National Research Center "Kurchatov Institute", Moscow 123098, Russia*
[32]*Kyoto University, Kyoto 606-8502, Japan*
[33]*Lawrence Livermore National Laboratory, Livermore, California 94550, USA*
[34]*Los Alamos National Laboratory, Los Alamos, New Mexico 87545, USA*
[35]*Department of Physics, Lund University, Box 118, SE-221 00 Lund, Sweden*
[36]*IPNL, CNRS/IN2P3, Univ Lyon, Université Lyon 1, F-69622 Villeurbanne, France*
[37]*University of Maryland, College Park, Maryland 20742, USA*
[38]*Department of Physics, University of Massachusetts, Amherst, Massachusetts 01003-9337, USA*
[39]*MATE, Laboratory of Femtoscopy, Károly Róbert Campus, H-3200 Gyöngyös, Mátraiút 36, Hungary*
[40]*Department of Physics, University of Michigan, Ann Arbor, Michigan 48109-1040, USA*
[41]*Mississippi State University, Mississippi State, Mississippi 39762, USA*
[42]*Muhlenberg College, Allentown, Pennsylvania 18104-5586, USA*
[43]*Nara Women's University, Kita-uoya Nishi-machi Nara 630-8506, Japan*
[44]*National Research Nuclear University, MEPhI, Moscow Engineering Physics Institute,*
Moscow, 115409, Russia
[45]*University of New Mexico, Albuquerque, New Mexico 87131, USA*
[46]*New Mexico State University, Las Cruces, New Mexico 88003, USA*
[47]*Physics and Astronomy Department, University of North Carolina at Greensboro,*
Greensboro, North Carolina 27412, USA
[48]*Department of Physics and Astronomy, Ohio University, Athens, Ohio 45701, USA*
[49]*Oak Ridge National Laboratory, Oak Ridge, Tennessee 37831, USA*
[50]*IPN-Orsay, Univ. Paris-Sud, CNRS/IN2P3, Université Paris-Saclay, BP1, F-91406 Orsay, France*
[51]*Peking University, Beijing 100871, People's Republic of China*
[52]*PNPI, Petersburg Nuclear Physics Institute, Gatchina, Leningrad region, 188300, Russia*
[53]*Pusan National University, Pusan 46241, Korea*
[54]*RIKEN Nishina Center for Accelerator-Based Science, Wako, Saitama 351-0198, Japan*
[55]*RIKEN BNL Research Center, Brookhaven National Laboratory, Upton, New York 11973-5000, USA*
[56]*Physics Department, Rikkyo University, 3-34-1 Nishi-Ikebukuro, Toshima, Tokyo 171-8501, Japan*
[57]*Saint Petersburg State Polytechnic University, St. Petersburg 195251, Russia*

[58]Department of Physics and Astronomy, Seoul National University, Seoul 151-742, Korea

[59]Chemistry Department, Stony Brook University, SUNY, Stony Brook, New York 11794-3400, USA

[60]Department of Physics and Astronomy, Stony Brook University, SUNY,
Stony Brook, New York 11794-3800, USA

[61]University of Tennessee, Knoxville, Tennessee 37996, USA

[62]Texas Southern University, Houston, Texas 77004, USA

[63]Department of Physics, Tokyo Institute of Technology, Oh-okayama, Meguro, Tokyo 152-8551, Japan

[64]Tomonaga Center for the History of the Universe, University of Tsukuba, Tsukuba, Ibaraki 305, Japan

[65]Vanderbilt University, Nashville, Tennessee 37235, USA

[66]Weizmann Institute, Rehovot 76100, Israel

[67]Institute for Particle and Nuclear Physics, Wigner Research Centre for Physics,
Hungarian Academy of Sciences (Wigner RCP, RMKI)
H-1525 Budapest 114, POBox 49, Budapest, Hungary

[68]Yonsei University, IPAP, Seoul 120-749, Korea

[69]Department of Physics, Faculty of Science, University of Zagreb,
Bijenička c. 32 HR-10002 Zagreb, Croatia

[70]Department of Physics, School of Natural Sciences, University of Zambia,
Great East Road Campus, Box 32379, Lusaka, Zambia

Reported here are transverse single-spin asymmetries (A_N) in the production of charged hadrons as a function of transverse momentum (p_T) and Feynman-x (x_F) in polarized $p^\uparrow + p$, $p^\uparrow + $ Al, and $p^\uparrow + $ Au collisions at $\sqrt{s_{NN}} = 200$ GeV. The measurements have been performed at forward and backward rapidity ($1.4 < |\eta| < 2.4$) over the range of 1.5 GeV/$c < p_T < 7.0$ GeV/c and $0.04 < |x_F| < 0.2$. A nonzero asymmetry is observed for positively charged hadrons at forward rapidity ($x_F > 0$) in $p^\uparrow + p$ collisions, whereas the $p^\uparrow + $ Al and $p^\uparrow + $ Au results show smaller asymmetries. This finding provides new opportunities to investigate the origin of transverse single-spin asymmetries and a tool to study nuclear effects in $p + A$ collisions.

I. INTRODUCTION

An understanding of transverse single-spin asymmetries (TSSAs) in transversely polarized proton-proton collisions ($p^\uparrow + p$) is crucial for disentangling the spin structure of the proton and parton dynamics within the proton. The analyzing power A_N is defined as the left-right asymmetry of the produced hadrons with respect to the spin direction of the polarized proton where the polarization direction is perpendicular to the beam direction. Since the 1970s, significant TSSAs in hadron (h) production ($p^\uparrow + p \to h + X$) have been measured at large Feynman-x ($x_F = 2p_L/\sqrt{s}$) for a wide range of collision energies up to 500 GeV [1–13]. Two approaches have been proposed to account for these large asymmetries. First, the transverse-momentum dependent (TMD) approach is based on TMD

[*]PHENIX Collaboration Spokesperson: akiba@rcf.rhic.bnl.gov
[†]Deceased.

parton distribution and fragmentation functions. It requires two scales, a hard-scattering energy scale Q and a soft scale k_T describing the transverse momentum of partons in the proton or of hadrons relative to the parent parton in hadronization process, with $k_T \ll Q$. In this framework, the possible origins of the asymmetry are the Sivers [14,15] and Collins [16] mechanisms. The Sivers mechanism describes the initial-state correlation between the spin of the transversely polarized proton and the parton transverse momentum, while in the final state the Collins mechanism introduces a correlation between the transverse spin of the fragmenting quark and transverse momentum of the final state hadron. The Collins mechanism convolves with the quark transversity distribution, which describes the quark transverse polarization inside a transversely polarized proton. Secondly, in the other framework, the collinear twist-3 factorization is applicable for observables with one large scale Q, which is usually represented by the particle transverse momentum p_T in reactions such as $p^\uparrow + p \to h + X$. In this framework, the asymmetry arises from a twist-3 multiparton correlation function and a twist-3 fragmentation function. Twist-3 multiparton correlation functions represent a spin dependence of the transverse motion of the parton inside a polarized proton [17–25].

Twist-3 fragmentation functions denote parton fragmentation effects during the formation of the final state hadrons. Recent calculations of the twist-3 contribution from parton fragmentation are shown to be important to describe the Relativistic Heavy Ion Collider (RHIC) results [26–28]. Also, a recent phenomenological study using both TMD and collinear twist-3 approaches demonstrates that TSSAs in Semi-Inclusive Deep Inelastic Scattering (SIDIS), Drell-Yan, e^+e^- annihilation, and proton-proton collisions have a common origin [29].

Recently, an exploration of the interplay of spin physics and small-x physics through the measurement of TSSAs in transversely polarized proton-nucleus collisions ($p^\uparrow + A$) has attracted attention, where x is the momentum fraction of a proton carried by the parton. In $p + A$ collisions, the properties of small-x gluons inside nuclei can be probed by measuring hadron production in the proton-going direction. The gluon density in the small-x region of the target nuclei is expected to increase significantly and it may be described by the color-glass-condensate (CGC) formalism [30]. The framework introduces a characteristic saturation scale Q_s which describes the color-charge density fluctuations, where $Q_{sA} \propto A^{1/3}$ for the target nucleus. In $p^\uparrow + A$ collisions, measuring TSSAs can be used as a probe for the saturation scale in the nucleus [31]. In addition, TSSAs in the forward region from $p^\uparrow + A$ collisions help to disentangle differing mechanisms and clarify the origin of the TSSA. Previous calculations of TSSAs incorporating gluon saturation at small-x suggest that TSSAs in $p^\uparrow + A$ may or may not be A-dependent, depending on the mechanisms involved [31–36]. On the experimental side, the A_N of positively charged hadrons at $0.1 < x_F < 0.2$ in PHENIX [37] and π^0 results at $0.2 < x_F < 0.7$ in STAR in $p^\uparrow + p$ and $p^\uparrow + A$ collisions have been reported

recently [38]. It should be noted that the kinematic region of the measurements presented here is outside of the expected CGC range, but considerations on the A-dependence of the various contributions might still be relevant.

This paper reports on measurements in 2015 of the transverse single-spin asymmetry for the production of charged hadrons ($h^\pm$) over the range of 1.5 GeV/c < p_T < 7.0 GeV/c and $0.04 < |x_F| < 0.2$ at forward and backward rapidity $(1.4 < |\eta| < 2.4)$ from transversely polarized proton-proton ($p^\uparrow + p$), proton-aluminum ($p^\uparrow + $ Al), and proton-gold ($p^\uparrow + $ Au) collisions at $\sqrt{s_{NN}} = 200$ GeV. Section II describes the experimental setup in PHENIX and the polarized beams at RHIC. The details of the analysis procedure are presented in Sec. III, and the result are shown in Sec. IV with discussions in Sec. V and finally, the summary in Sec. VI.

II. EXPERIMENTAL SETUP

A. The PHENIX experiment

The PHENIX detector [39] is equipped with central arms at midrapidity, and muon arms at backward and forward rapidity. The muon arms cover the pseudorapidity range $1.2 < \eta < 2.4$ (north arm) and $-2.2 < \eta < -1.2$ (south arm) and the full azimuthal angle ($\Delta\phi = 2\pi$) [40]. The side view of the PHENIX detector including muon arms during the 2015 run is shown in Fig. 1. Muons and hadrons from the interaction region pass through a hadron absorber of 7.5 nuclear interaction lengths (λ_I). Surviving muons and hadrons reach a muon tracker (MuTr) composed of three stations of cathode-strip readout tracking chambers mounted inside conical-shaped muon magnets. The momentum of a charged particle is measured with the MuTr. The muon identifier (MuID) behind the MuTr is
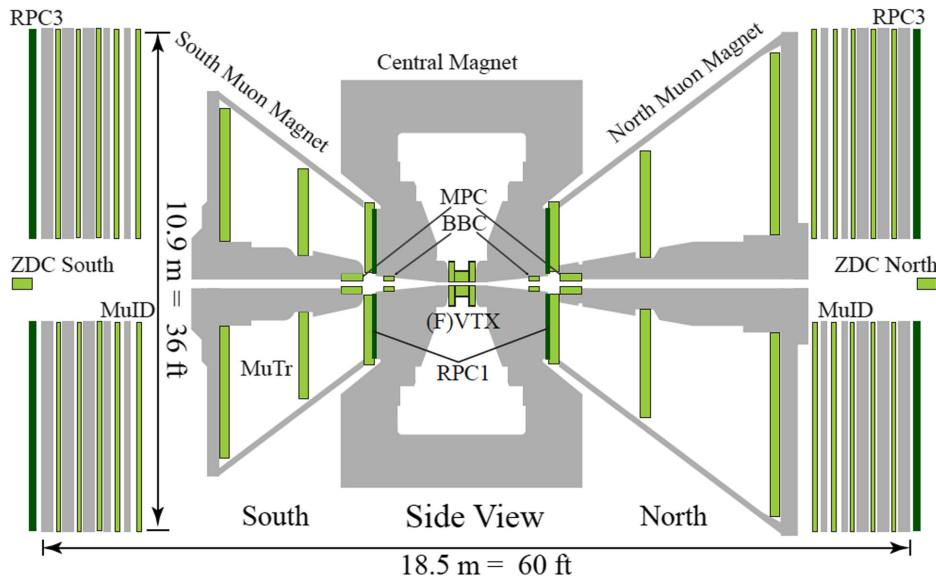

FIG. 1.   Side view of the PHENIX detector in 2015.

composed of five layers (labeled from Gap0 to Gap4) of proportional tube planes combined with an absorber plane ($\approx 1\lambda_I$), respectively. The MuID provides identification of hadrons and muons by measuring penetration depth. Muons of momentum larger than 3 GeV/c penetrate all layers while charged hadrons are mostly stopped at the intermediate layers (Gap2 and Gap3) [41].

The beam-beam counters (BBC) are located at $z = \pm 144$ cm from the interaction point and cover the pseudorapidity range $3.1 < |\eta| < 3.9$ and full azimuthal angle [42]. Each BBC comprises 64 quartz Čerenkov counters. The BBC detects charged particles and provides z-vertex position with a resolution of ≈ 2 cm in $p + p$ collisions. The BBC is also used to categorize events with energy deposition in terms of centrality for collisions with ion beam. In the case of $p^\uparrow + {\rm Au}$ and $p^\uparrow + {\rm Al}$ collisions, energy deposition in the A-going direction is used for determining centrality. In addition, the BBC serves as a luminosity monitor.

The minimum-bias trigger provided by the BBC requires at least one hit in both directions. The BBC trigger efficiency is 55% in $p^\uparrow + p$, 72% in $p^\uparrow + {\rm Al}$, and 84% in $p^\uparrow + {\rm Au}$ collisions. The MuID provides a trigger to select events containing hadron or muon tracks by requiring at least one MuID track reaching Gap2, Gap3, or Gap4. For charged hadrons, events with track candidates having a hit at the Gap2 or Gap3 but no hit at the Gap4 are selected. The new readout electronics for the MuTr allow to trigger events with high momentum ($p_T > 3$ GeV/c) tracks by requiring maximum bending at the middle plane less than three MuTr cathode strips [43].

B. RHIC polarized beams

RHIC is the world's first and only polarized proton collider, located at Brookhaven National Laboratory, comprising two countercirculating storage rings. In each ring, as many as 120 bunches of heavy ions or polarized protons can be accelerated up to 100 GeV for heavy ions and 255 GeV for polarized protons. During the 2015 run period, data from the collisions of vertically polarized protons and ions ($p^\uparrow + p$, $p^\uparrow + {\rm Al}$, and $p^\uparrow + {\rm Au}$) at $\sqrt{s_{NN}} = 200$ GeV were recorded. Each beam bunch of 106 ns interval has a separate polarization (up or down). The predetermined polarization patterns for every eight bunches were changed at each fill to minimize systematic effects due to time dependence of the detector and accelerator performance. In the $p^\uparrow + A$ run, the counterclockwise direction was selected for ion beams where the beam points towards the south muon arm.

The average polarization of the proton beam was 58% (clockwise beam) and 57% (counterclockwise beam) for $p^\uparrow + p$ collisions, 58% for $p^\uparrow + {\rm Al}$ collisions, and 61% for $p^\uparrow + {\rm Au}$ collisions with 3% relative uncertainty from the polarization normalization [44].

III. DATA ANALYSIS

A. Dataset

The integrated luminosity of the data in this analysis is 37 pb^{-1} from $p^\uparrow + p$, 593 nb^{-1} from $p^\uparrow + {\rm Al}$, and 112 nb^{-1} from $p^\uparrow + {\rm Au}$ collisions. The data was recorded using the hadron trigger in combination with the BBC trigger. The hadron trigger selected high-momentum tracks when the last MuID gap for a track pass through is MuID Gap2 or Gap3, with the bending at the middle plane of MuTr being less than three cathode strips [43].

B. Charged hadron selection

Among the reconstructed tracks stopped at MuID Gap2 or Gap3 are low-momentum muons from light hadron decays. From full GEANT4 simulation studies, such background is significantly suppressed ($< 5\%$) after applying a cut $p_z > 3.5$ GeV/c [45]. The additional track quality cuts are listed in Table I with numerical values shown for Gap3 tracks at $1.25 < p_T < 1.5$ GeV/c. The distance and angular difference between the extrapolated MuTr track and the MuID track at the first MuID plane's z position are called DG0 and DDG0. The distance between the interaction point and a projected position of a MuID track at $z = 0$ is $r_{\rm ref}$. The number of hits in a MuTr track and χ^2 per degree of freedom ($\chi^2_{\rm MuTr}/ndf$) are also included in the track quality cut. The quality cuts are p_T dependent except for the number of hits in a MuTr track and $\chi^2_{\rm MuTr}/ndf$. The polar scattering angle of a track inside the absorber scaled by the momentum is $p \cdot (\theta_{\rm MuTr} - \theta_{\rm vtx})$. $\theta_{\rm vtx}$ is the polar angle at the collision vertex with the momentum vector at the vertex, obtained by a track fit from the MuTr and MuID to the primary vertex. $\theta_{\rm MuTr}$ is the polar angle at the MuTr Station 1 of the reconstructed track using the MuTr so that the $p \cdot (\theta_{\rm MuTr} - \theta_{\rm vtx})$ corresponds to the polar scattering angle of a track inside the absorber scaled by the momentum. Cuts applied to $p \cdot (\theta_{\rm MuTr} - \theta_{\rm vtx})$ and χ^2 at $z_{\rm vtx}$ are effective for rejecting muons decayed inside the absorber.

An estimation of the particle composition in the measured charged hadron sample was developed in [41,46]. Based on PYTHIA [47] and HIJING [48] event generators. Charged hadron spectra measured at midrapidity in $p + p$ and $d + {\rm Au}$ at RHIC [49–51] were extrapolated to the PHENIX muon arm rapidity ($1.2 < \eta < 2.4$) for $p + p$,

TABLE I. Track selection cuts for tracks stopped at MuID Gap3 for a p_T bin $1.25 < p_T < 1.5$ GeV/c.

DG0 < 29 cm (south), 18.5 cm (north)
DDG0 < 12 deg.
$r_{\rm ref}$ < 140 cm (south), 159 cm (north)
Number of hits in MuTr > 10, $\chi^2_{\rm MuTr}/ndf$ < 20
$p \cdot (\theta_{\rm MuTr} - \theta_{\rm vtx})$ < 0.35 rad $\cdot$ GeV/c
χ^2 of track projection to $z_{\rm vtx}$ < 8.5

FIG. 2. Estimation of K/π ratios at the collision vertex (Generation) and K/π ratios for reconstructed muon arm tracks in in the GEANT4 simulation (Reconstruction) for $p + p$ collisions. The variations from the different physics list in the GEANT4 simulation are shown as the bands on the reconstructed K/π ratios. According to the simulation, the reconstructed particle composition is modified compared to the generated one due to interaction with the detector material.
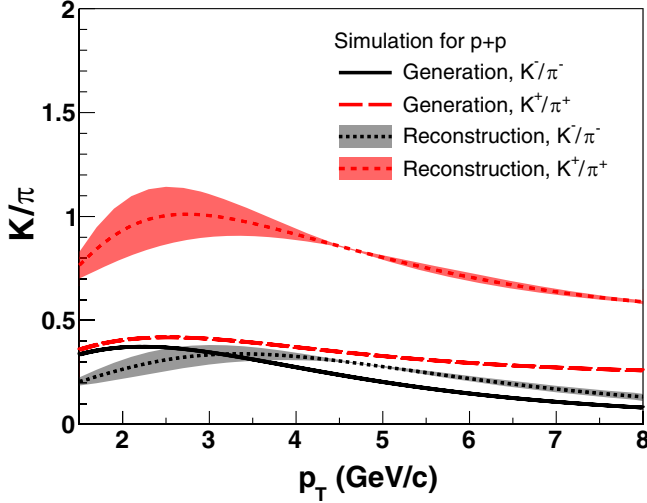

FIG. 3. Estimation of K/π ratios at the collision vertex (Generation) and K/π ratios for reconstructed muon arm tracks in in the GEANT4 simulation (Reconstruction) for $p + A$ collisions. The variations from the different physics lists in the GEANT4 simulation are shown as the bands on the reconstructed K/π ratios. According to the simulation, the reconstructed particle composition is modified compared to the generated one due to interaction with the detector material.

$p +$ Al, and $p +$ Au collisions. According to a GEANT4 [52] detector simulation (release 10.0.p02), the initial particle composition is modified due to interaction with the detector material including the front absorber. The reconstructed charged hadrons are mostly $K^{\pm}$ and $\pi^{\pm}$ where others (p, $\bar{p}$) are less than 10%. The estimated K/π ratios at the collision vertex and reconstructed ratios from the simulation are shown in Fig. 2 for $p + p$ collisions and Fig. 3 for $p + A$ collisions. In both $p + p$ and $p + A$ collisions, the reconstructed K^{-} are more suppressed than K^{+} by the front absorber material due to its larger cross section with protons [53]. Momentum smearing also changes the shape of the ratios. Among the GEANT4 physics lists [54], the default used is the QGSP-BERT, which to simulate hadronic interactions applies the quark-gluon string model for high-energy and the Bertini cascade model for low-energy hadrons. To estimate possible variations, the FTFP-BERT and QGSP-BIC physics lists are used where the FTF model uses the FRITIOF description of string excitation and fragmentation and BIC uses the binary cascade model. The variations from the different physics lists in the GEANT4 simulation are shown in Figs. 2 and 3 as bands on the reconstructed K/π ratios.

C. Determination of the TSSA

The unbinned maximum-likelihood method was used to extract the TSSA (A_N) in this study. It was established in the previous study which used the same detectors [37,55,56]. The method is robust even for low-statistics data compared to binned approaches. The extended log-likelihood $\log \mathcal{L}$ is defined as
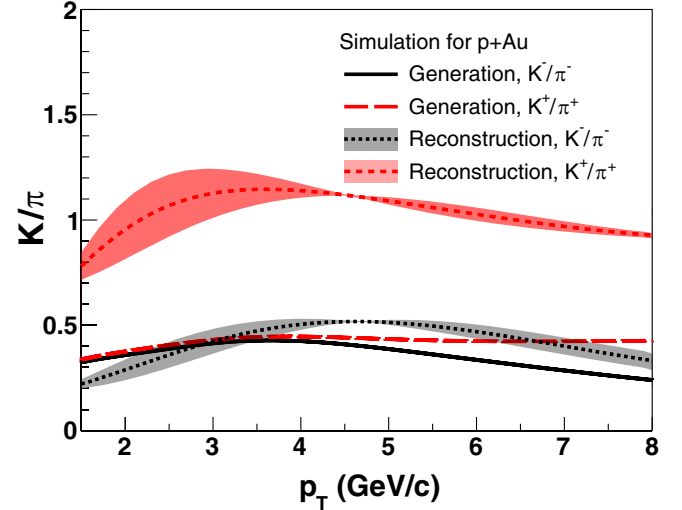
$$\log \mathcal{L} = \sum_i \log(1 + P \cdot A_N \sin(\phi_{\text{pol}} - \phi_h^i)) + \text{constant},$$

$$(1)$$

where P is the proton beam polarization and ϕ_h^i is the azimuthal angle of the ith hadron with respect to the incoming polarized-proton-beam direction. The ϕ_{pol} is the azimuthal angle for the beam polarization direction, which takes the values of $+\frac{\pi}{2}/-\frac{\pi}{2}$ for $\uparrow/\downarrow$ polarized beam bunches in 2015. The A_N is chosen to be the value which maximizes $\log \mathcal{L}$. The statistical uncertainty of the log-likelihood estimator is calculated from the second derivative of $\mathcal{L}$ with respect to A_N,

$$\sigma^2(A_N) = \left(-\frac{\partial^2 \mathcal{L}}{\partial A_N^2}\right)^{-1}. \qquad (2)$$

In $p + p$ collisions, both beams were polarized. The A_Ns were measured separately for each beam and turned out to be consistent with each other. They were averaged for the final asymmetry.

The A_N is checked with the azimuthal-fitting method used in previous analyses [12,37,55,56] based on the polarization formula [57]:

$$A_N(\phi) = \frac{\sigma^{\uparrow}(\phi) - \sigma^{\downarrow}(\phi)}{\sigma^{\uparrow}(\phi) + \sigma^{\downarrow}(\phi)} = \frac{1}{P} \cdot \frac{N^{\uparrow}(\phi) - R \cdot N^{\downarrow}(\phi)}{N^{\uparrow}(\phi) + R \cdot N^{\downarrow}(\phi)}, \qquad (3)$$

where $A_N(\phi)$ indicates the simple-count-based transverse single-spin asymmetry calculated for each of 16 azimuthal
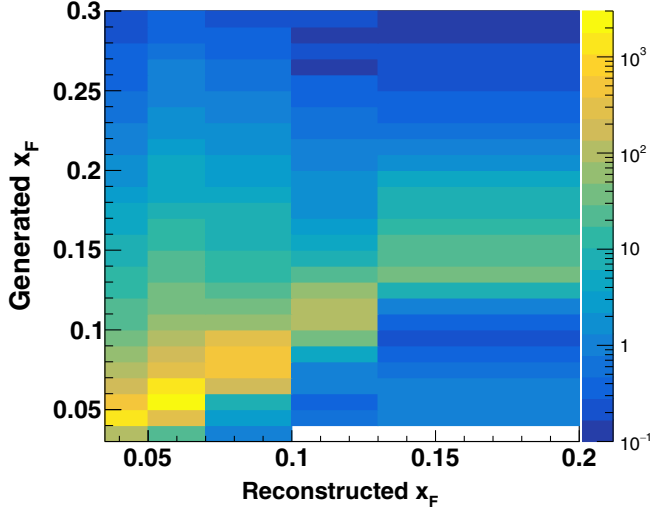
FIG. 4.   The distribution of generated x_F for reconstructed x_F bins from GEANT4 simulation in $p + p$ collisions.

ϕ-bins; $\sigma^\uparrow$, $\sigma^\downarrow$ represent cross sections; and $N^\uparrow$, $N^\downarrow$ are yields for each polarization of spin up ($\uparrow$) or down ($\downarrow$). $R = L^\uparrow/L^\downarrow$ is the ratio of luminosities (relative luminosity) between bunches with spin up and spin down where the luminosity is determined by sampled counts from minimum-bias triggers for the corresponding spin orientation. The A_N in this method is calculated from the fit of $A_N(\phi)$ distributions using a function $A_N \cdot \sin(\phi_{\text{pol}\uparrow} - \phi)$ where $\phi_{\text{pol}\uparrow} = \pi/2$ indicates the azimuthal direction of upward polarized bunches. The difference of the A_N's for this method and the maximum-likelihood method is conservatively included in the systematic uncertainty.

The interactions between particles and material prior to being detected by the MuTr, and the finite resolution for momentum and azimuthal angle ϕ, may result in a kinematic smearing effect for the A_N results. The full GEANT4 simulation is used to correct this effect. The effect from ϕ smearing was found to be negligible.

The momentum smearing is represented in Fig. 4, where the generated x_F distribution for reconstructed x_F bin is shown. The momentum smearing effect is corrected by resolving a set of linear equations which connect A_N for reconstructed x_F (p_T) bins (A_N^{reco}) and A_N for true (generated) x_F (p_T) bins (A_N^{true}),

$$A_N^{\text{reco},m} = \sum_i f^{i \to m} \cdot A_N^{\text{true},i}, \qquad (4)$$

where $A_N^{\text{true},i}$ represents A_N for the ith true momentum (x_F, p_T) bin and $A_N^{\text{reco},m}$ is A_N for the reconstructed momentum in the mth momentum bin. $f^{i \to m}$ is the fraction of charged hadrons reconstructed in the mth momentum bin from the ith true (generated) momentum bin in the simulation. A_N^{reco} is measured including an underflow and overflow bin for $0.035 < x_F < 0.3$ and $1.25 \text{ GeV}/c < p_T < 15 \text{ GeV}/c$,

and then A_N^{true} is calculated for $0.04 < x_F < 0.2$ and $1.5 \text{ GeV}/c < p_T < 7 \text{ GeV}/c$. The difference between A_N^{reco} and A_N^{true} was found to be small, and was conservatively included in systematic uncertainties. The variation of A_N due to muon contribution is minimal (< 0.0005) and not included in the systematic uncertainty.

IV. RESULTS

A. Results in proton-proton collisions

The TSSAs in the production of charged hadrons at $1.2 < |\eta| < 2.4$ in transversely-polarized proton-proton collisions ($p^\uparrow + p$) are shown in Fig. 5 as a function of p_T and in Fig. 6 as a function of x_F. The results are listed in Tables II–V. In the tables, δA_N^{stat} is the statistical uncertainty, and δA_N^{syst} is the total systematic uncertainty. The systematic uncertainty is obtained from the quadratic sum of two components ($\delta A_N^{\text{method}}$ and $\delta A_N^{\text{smear}}$). As explained in the previous section, $\delta A_N^{\text{method}}$ is the difference between the two methods of determining A_N, while $\delta A_N^{\text{smear}}$ is the difference caused by the momentum migration correction (Eq. (4). Three different physics lists are tested in the correction and the variation among them is negligible.

On the panel (a) of Fig. 5, A_N at backward rapidity ($x_F < 0$) for charged hadrons is consistent with zero within uncertainty. On the panel (b), A_N at forward rapidity ($x_F > 0$) is positive for positively charged hadrons. Positive asymmetry is also shown in the x_F-binned result in Fig. 6. A_N for positively charged hadrons at $x_F > 0$ shows an increasing trend with respect to x_F. The result for negatively charged hadrons shows some indication of negative A_N around $x_F > 0.07$.

The previous results at RHIC energies with larger $|x_F|$ and $|\eta|$ than this measurement showed positive A_N for π^+,
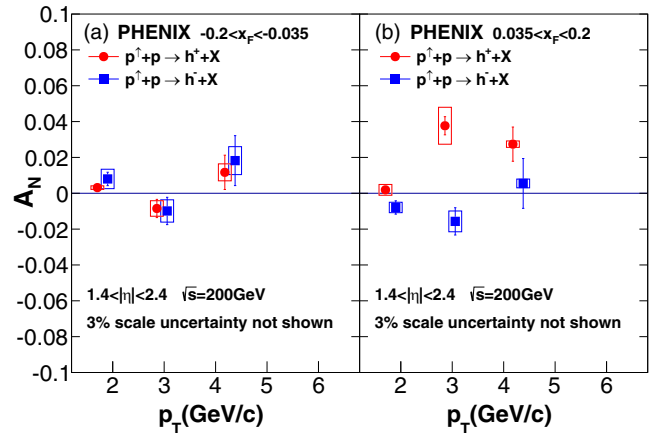

FIG. 5. A_N of charged hadrons from $p^\uparrow + p$ collisions as a function of p_T in the (a) backward ($x_F < 0$,) and (b) forward ($x_F > 0$) regions. Vertical bars (boxes) represent statistical (systematic) uncertainties. Points are shifted by $p_T = +0.2 \text{ GeV}/c$ for negatively charged hadrons. A scale uncertainty from the polarization (3%) is not included.
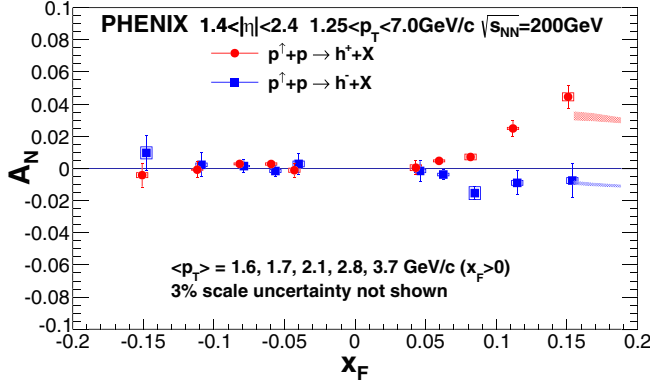
FIG. 6. A_N of charged hadrons from $p^\uparrow + p$ collisions as a function of x_F, where $x_F > 0$ is along the direction of the polarized proton. Vertical bars (boxes) represent statistical (systematic) uncertainties. Points are shifted by $x_F = +0.003$ for negatively charged hadrons. Dotted bands represent twist-3 model calculations [28] by varying the K/π ratio by $\pm 30\%$ of the central value. A scale uncertainty from the polarization (3%) is not included.

$K^\pm$ and negative A_N for π^- at $x_F > 0$ [7,9]. In this measurement, the result for h^+ is comparable with A_N for π^+, K^+. A_N for h^+ is increasing as a function of x_F at $x_F > 0$ and is consistent with zero at $x_F < 0$. π^- and K^- in the previous measurements showed the opposite sign of A_N at forward rapidity. Therefore, one may expect the A_N for h^- has been partially canceled and this can explain the smaller size of A_N for h^- at $x_F > 0$ in Fig. 6. This is also confirmed in twist-3 model calculations shown in Fig. 6. The dotted bands in Fig. 6 are obtained from K/π ratios in the simulation combined with theoretical A_N for charged pions and kaons from twist-3 calculation for $x_F > 0.15$ [28], which describes previous RHIC results at forward rapidity [7,9]. In addition, the effect of the K/π production ratio variation is tested for a relative $\pm 30\%$ variation and the width of the band shows the possible variation of A_N mixture for h^+ and h^-. The variation of the K/π production ratio from different GEANT4 physics lists shown in Fig. 2 is much smaller than the relative $\pm 30\%$ that was considered.

B. Results in proton-nucleus collisions

The A_N results of charged hadrons in proton-nucleus collisions ($p^\uparrow + Al$ and $p^\uparrow + Au$) are shown in Figs. 7–9 with $p^\uparrow + p$ results and listed in Tables VI–IX for $p^\uparrow + Al$ and Tables X–XIII for $p^\uparrow + Au$. Results at $x_F < 0$ in all collision systems ($p^\uparrow + p$, $p^\uparrow + A$) are close to zero; the combined A_N are within 1.5σ from zero where σ is total uncertainty. Results for negatively charged hadrons from $p^\uparrow + Al$ and $p^\uparrow + Au$ collisions shown in Figs. 7 and 9 are also close to zero in terms of the total uncertainty; the combined A_N are within 1.2σ from zero. In contrast, A_N in $p^\uparrow + p$ collisions shows some indication of a negative asymmetry at $p_T < 3.5$ GeV/c on panel (b) ($x_F > 0$) of
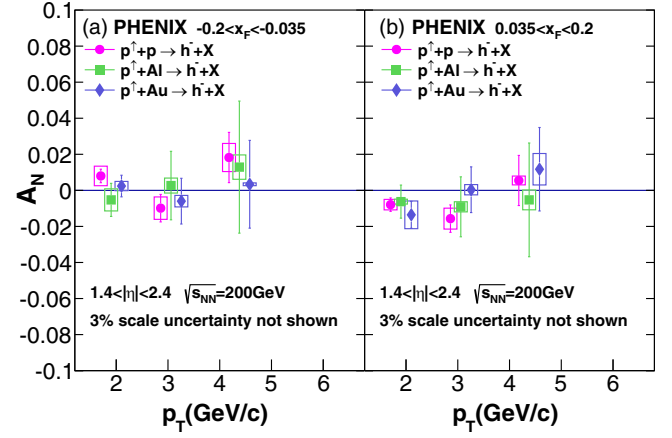

FIG. 7. A_N of negatively charged hadrons from $p^\uparrow + p$, $p^\uparrow + Al$, and $p^\uparrow + Au$ collisions as a function of p_T in the (a) backward ($x_F < 0$) and (b) forward ($x_F > 0$) regions. Vertical bars (boxes) represent statistical (systematic) uncertainties. Points are shifted by $p_T = +0.02$ ($+0.04$) GeV/c for $p^\uparrow + Al$ ($p^\uparrow + Au$) results. A scale uncertainty from the polarization (3%) is not included.

Fig. 7 and at $0.07 < x_F < 0.10$ on panel (a) of Fig. 9. However, the difference of A_N between $p^\uparrow + Au$ and $p^\uparrow + p$ is not significant to state any modification of $|A_N|$ in $p^\uparrow + Au$ compared to $p^\uparrow + p$ results.

The A_N for positively charged hadrons at $x_F > 0$ in $p^\uparrow + Au$ collisions is consistent with zero while the results for $p^\uparrow + p$ represents a positive asymmetry on panel (b) in Fig. 8 and on panel (b) in Fig. 9. The $p^\uparrow + Al$ results for h^+ at $x_F > 0$ show some indication of a positive asymmetry, which is smaller than in $p^\uparrow + p$ collisions.

FIG. 8. A_N of positively charged hadrons from $p^\uparrow + p$, $p^\uparrow + Al$, and $p^\uparrow + Au$ collisions as a function of p_T in the (a) backward ($x_F < 0$) and (b) forward ($x_F > 0$) regions. Vertical bars (boxes) represent statistical (systematic) uncertainties. Points are shifted by $p_T = +0.02$ ($+0.04$) GeV/c for $p^\uparrow + Al$ ($p^\uparrow + Au$) results. A scale uncertainty from the polarization (3%) is not included.

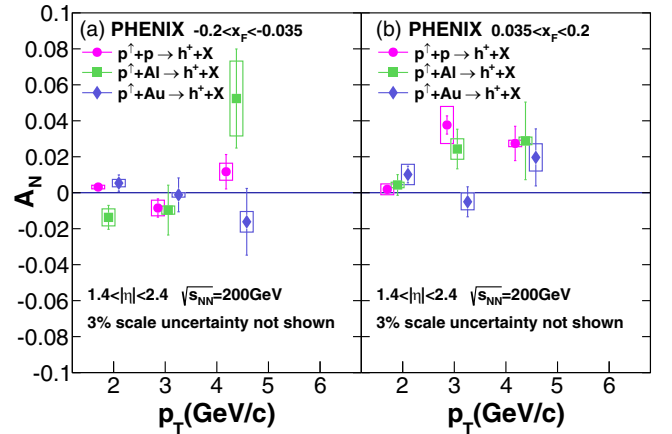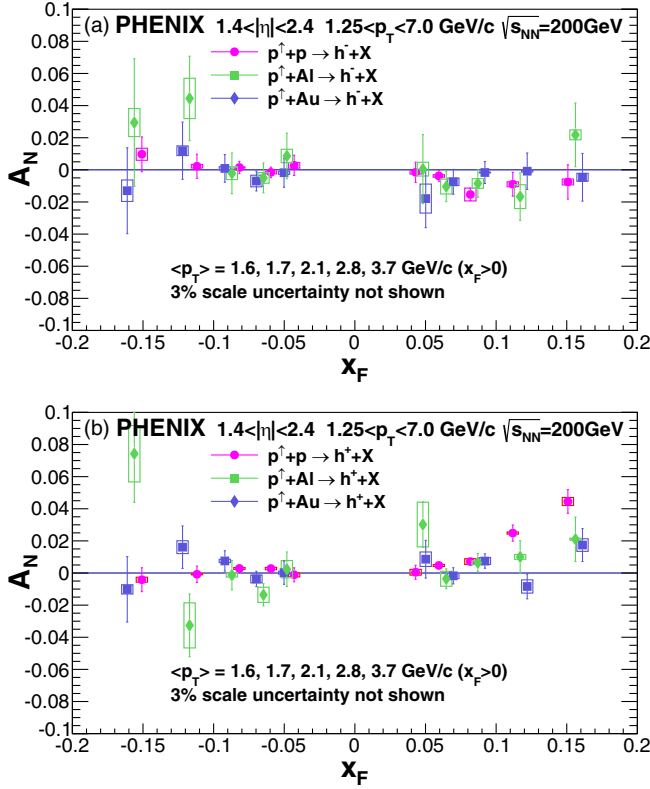FIG. 9. A_N of (a) negatively charged hadrons and (b) positively charged hadrons from $p^\uparrow + p$, $p^\uparrow + Al$, and $p^\uparrow + Au$ collisions as a function of x_F, where $x_F > 0$ is along the direction of the polarized proton. Vertical bars (boxes) represent statistical (systematic) uncertainties. Points are shifted by $x_F = -0.01$, $-0.005, +0.005, +0.01(-0.005, -0.003, +0.003, +0.005)$ at $-0.2 < x_F < -0.05, -0.05 < x_F < 0.04, 0.04 < x_F < 0.05, 0.05 < x_F < 0.2$, respectively for $p^\uparrow + Au$ ($p^\uparrow + Al$) results. A scale uncertainty from the polarization (3%) is not included.

V. DISCUSSION

The results for the production of positively charged hadrons (h^+) in $p^\uparrow + p$ collisions agree with a trend with other RHIC data where A_N for π^+ and K^+ is positive and increasing with respect to x_F in the forward region ($x_F > 0$) [7,9]. The results for A_N for negatively charged hadrons (h^-) range from slightly negative to zero at $x_F > 0$; this may be caused by cancellation between positive asymmetry for K^- and negative asymmetry for π^- shown in RHIC data at larger x_F [7,9]. These agree with the trend of the theoretical calculation at $x_F > 0.15$ [28]. In all collision systems, A_N at backward rapidity ($x_F < 0$) is close to zero asymmetry in terms of the total uncertainty, which also has been shown in previous RHIC measurements in $p^\uparrow + p$ collisions [8,9,11]. The A_N of positively charged hadrons at $0.1 < x_F < 0.2$ in $p^\uparrow + Al$ and $p^\uparrow + Au$ is smaller than in $p^\uparrow + p$. However, the total uncertainty of $p^\uparrow + Al$ results is too large to provide clear separation from $p^\uparrow + p$ or $p^\uparrow + Au$ results while $p^\uparrow + Au$ shows nuclear dependence.

Recent calculations using collinear factorization on polarized proton ($p^\uparrow$) and the CGC framework on nuclear target (A) [33] predicted that the A_N of inclusive hadrons at forward rapidity in $p^\uparrow + A$ collisions has two contributions where one is A-independent and the other is $A^{-1/3}$-dependent [35,36,58,59]. However, the $A^{-1/3}$-dependent term is dominant for p_T less than Q_s and A-independent term is dominant for higher p_T. In the kinematics of this measurement according to a recent calculation [59], $Q_s^{Au} \approx 0.9$ GeV whereas our measurements correspond to $\langle p_T \rangle \approx 2.9$ GeV/c at $0.1 < x_F < 0.2$. An approach using lensing mechanism predicts that A_N decreases as the atomic number of the target (A) increases for k_T below or near Q_s [60]. A recent STAR result of π^0 in the more forward region at $2.6 < \eta < 4.0$, $p_T > 1.5$ GeV/c, and $0.2 < x_F < 0.7$ in $p^\uparrow + p$ and $p^\uparrow + Au$ collisions shows a smaller A-dependence [38] than what is observed here. Given that our measurement and that from STAR used different kinematic ranges and hadron species, further detailed studies of various observables within a wide kinematic range will be informative on the origin of A_N and its interplay with small-x phenomena.

VI. SUMMARY

Reported here are the transverse single-spin asymmetry (A_N) of positively and negatively charged hadrons ($h^\pm$) in forward and backward rapidity ($1.4 < |\eta| < 2.4$) over the range of 1.5 GeV/c < p_T < 7.0 GeV/c and $0.04 < |x_F| < 0.2$ from transversely polarized proton-proton ($p^\uparrow + p$) and proton-nucleus ($p^\uparrow + A$) collisions. The results at $x_F < 0$ are close to zero at all systems. In $x_F > 0$, negative charged hadron results show small to zero A_N in $p^\uparrow + p$ collisions and nearly zero A_N in $p^\uparrow + A$ collisions. A_N for positively charged hadrons increases to positive values as x_F increases in $p^\uparrow + p$ collisions, but $p^\uparrow + Au$ results show suppression of A_N at $0.1 < x_F < 0.2$ compared to the $p^\uparrow + p$ result. The results will aid in understanding of the origin of A_N and offer a tool to investigate nuclear effects and phenomena in small x.

ACKNOWLEDGMENTS

APPENDIX: DATA TABLES

Tables II–V list the TSSAs in the production of charged hadrons at $1.2 < |\eta| < 2.4$ in transversely-polarized proton-proton collisions $(p^\uparrow + p)$ that are shown in Fig. 5 as a function of p_T and in Fig. 6 as a function of x_F. See further details in Sec. III A. Tables VI–IX for $p^\uparrow + $ Al and Tables X–XIII for $p^\uparrow + $ Au. list the A_N results of charged hadrons in proton-nucleus collisions ($p^\uparrow + $ Al and $p^\uparrow + $ Au) that are shown in Figs. 7–9 with $p^\uparrow + p$ results. See further details in Sec. III 'B.

TABLE II. Data table of A_N for negatively charged hadron (h^-) in transversely-polarized $p + p$ collisions as a function of p_T.

$p_T(\text{GeV}/c)$	A_N	δA_N^{stat}	δA_N^{syst}	$\delta A_N^{\text{method}}$	$\delta A_N^{\text{smear}}$
Forward ($x_F > 0$)					
(1.50, 2.50)	−0.008	±0.004	±0.003	±0.001	±0.003
(2.50, 3.50)	−0.016	±0.008	±0.006	±0.001	±0.006
(3.50, 7.00)	0.005	±0.014	±0.002	±0.002	±0.002
Backward ($x_F < 0$)					
(1.50, 2.50)	0.008	±0.004	±0.005	±0.000	±0.005
(2.50, 3.50)	−0.010	±0.008	±0.006	±0.001	±0.006
(3.50, 7.00)	0.018	±0.014	±0.008	±0.001	±0.008

TABLE III. Data table of A_N for positively charged hadron (h^+) in transversely-polarized $p + p$ collisions as a function of p_T.

$p_T(\text{GeV}/c)$	A_N	δA_N^{stat}	δA_N^{syst}	$\delta A_N^{\text{method}}$	$\delta A_N^{\text{smear}}$
Forward ($x_F > 0$)					
(1.50, 2.50)	0.002	±0.002	±0.003	±0.000	±0.003
(2.50, 3.50)	0.038	±0.005	±0.010	±0.001	±0.010
(3.50, 7.00)	0.027	±0.010	±0.002	±0.001	±0.002
Backward ($x_F < 0$)					
(1.50, 2.50)	0.003	±0.002	±0.001	±0.001	±0.001
(2.50, 3.50)	−0.008	±0.005	±0.004	±0.001	±0.004
(3.50, 7.00)	0.012	±0.010	±0.005	±0.001	±0.004

TABLE IV. Data table of A_N for negatively charged hadron (h^-) in transversely-polarized $p + p$ collisions as a function of x_F.

x_F	A_N	δA_N^{stat}	δA_N^{syst}	$\delta A_N^{\text{method}}$	$\delta A_N^{\text{smear}}$
(−0.200, −0.130)	0.010	±0.011	±0.004	±0.003	±0.002
(−0.130, −0.100)	0.002	±0.008	±0.001	±0.001	±0.000
(−0.100, −0.070)	0.001	±0.004	±0.000	±0.000	±0.000
(−0.070, −0.050)	−0.002	±0.003	±0.001	±0.000	±0.001
(−0.050, −0.040)	0.003	±0.006	±0.002	±0.001	±0.002
(0.040, 0.050)	−0.002	±0.006	±0.001	±0.000	±0.001
(0.050, 0.070)	−0.004	±0.003	±0.001	±0.000	±0.001
(0.070, 0.100)	−0.015	±0.004	±0.004	±0.001	±0.004
(0.100, 0.130)	−0.009	±0.007	±0.002	±0.000	±0.001
(0.130, 0.200)	−0.008	±0.011	±0.002	±0.001	±0.001

TABLE V. Data table of A_N for positively charged hadron (h^+) in transversely-polarized $p + p$ collisions as a function of x_F.

x_F	A_N	δA_N^{stat}	δA_N^{syst}	$\delta A_N^{\text{method}}$	$\delta A_N^{\text{smear}}$
(−0.200, −0.130)	−0.004	±0.007	±0.002	±0.002	±0.000
(−0.130, −0.100)	−0.001	±0.005	±0.000	±0.000	±0.000
(−0.100, −0.070)	0.003	±0.003	±0.001	±0.000	±0.000
(−0.070, −0.050)	0.003	±0.002	±0.001	±0.001	±0.000
(−0.050, −0.040)	−0.001	±0.004	±0.001	±0.000	±0.001
(0.040, 0.050)	0.000	±0.004	±0.002	±0.001	±0.002
(0.050, 0.070)	0.005	±0.002	±0.001	±0.000	±0.001
(0.070, 0.100)	0.007	±0.003	±0.002	±0.000	±0.002
(0.100, 0.130)	0.025	±0.005	±0.001	±0.001	±0.000
(0.130, 0.200)	0.045	±0.007	±0.002	±0.001	±0.002

TABLE VI. Data table of A_N for negatively charged hadron (h^-) in transversely-polarized $p + $ Al collisions as a function of p_T.

$p_T(\text{GeV}/c)$	A_N	δA_N^{stat}	δA_N^{syst}	$\delta A_N^{\text{method}}$	$\delta A_N^{\text{smear}}$
Forward ($x_F > 0$)					
(1.50, 2.50)	−0.006	±0.009	±0.001	±0.001	±0.001
(2.50, 3.50)	−0.009	±0.017	±0.003	±0.002	±0.002
(3.50, 7.00)	−0.005	±0.032	±0.006	±0.002	±0.005
Backward ($x_F < 0$)					
(1.50, 2.50)	−0.005	±0.009	±0.006	±0.001	±0.006
(2.50, 3.50)	0.003	±0.019	±0.004	±0.004	±0.002
(3.50, 7.00)	0.013	±0.037	±0.007	±0.002	±0.007

TABLE VII. Data table of A_N for positively charged hadron (h^+) in transversely-polarized $p + $ Al collisions as a function of p_T.

$p_T(\text{GeV}/c)$	A_N	δA_N^{stat}	δA_N^{syst}	$\delta A_N^{\text{method}}$	$\delta A_N^{\text{smear}}$
		Forward ($x_F > 0$)			
(1.50, 2.50)	0.004	±0.006	±0.002	±0.002	±0.000
(2.50, 3.50)	0.024	±0.011	±0.006	±0.001	±0.006
(3.50, 7.00)	0.029	±0.022	±0.002	±0.001	±0.002
		Backward ($x_F < 0$)			
(1.50, 2.50)	−0.014	±0.007	±0.005	±0.001	±0.005
(2.50, 3.50)	−0.010	±0.014	±0.002	±0.001	±0.002
(3.50, 7.00)	0.052	±0.028	±0.021	±0.004	±0.020

TABLE VIII. Data table of A_N for negatively charged hadron (h^-) in transversely-polarized $p + $ Al collisions as a function of x_F.

x_F	A_N	δA_N^{stat}	δA_N^{syst}	$\delta A_N^{\text{method}}$	$\delta A_N^{\text{smear}}$
(−0.200, −0.130)	0.029	±0.040	±0.009	±0.000	±0.009
(−0.130, −0.100)	0.044	±0.026	±0.013	±0.006	±0.011
(−0.100, −0.070)	−0.002	±0.013	±0.004	±0.001	±0.004
(−0.070, −0.050)	−0.005	±0.009	±0.003	±0.001	±0.003
(−0.050, −0.040)	0.009	±0.014	±0.004	±0.000	±0.004
(0.040, 0.050)	0.000	±0.021	±0.004	±0.003	±0.003
(0.050, 0.070)	−0.010	±0.009	±0.005	±0.002	±0.004
(0.070, 0.100)	−0.008	±0.009	±0.003	±0.000	±0.003
(0.100, 0.130)	−0.017	±0.015	±0.007	±0.002	±0.007
(0.130, 0.200)	0.022	±0.020	±0.003	±0.000	±0.003

TABLE IX. Data table of A_N for positively charged hadron (h^+) in transversely-polarized $p + $ Al collisions as a function of x_F.

x_F	A_N	δA_N^{stat}	δA_N^{syst}	$\delta A_N^{\text{method}}$	$\delta A_N^{\text{smear}}$
(−0.200, −0.130)	0.074	±0.030	±0.018	±0.005	±0.017
(−0.130, −0.100)	−0.033	±0.020	±0.014	±0.004	±0.014
(−0.100, −0.070)	−0.001	±0.009	±0.001	±0.001	±0.001
(−0.070, −0.050)	−0.014	±0.007	±0.005	±0.001	±0.005
(−0.050, −0.040)	0.002	±0.011	±0.005	±0.002	±0.005
(0.040, 0.050)	0.030	±0.014	±0.014	±0.001	±0.014
(0.050, 0.070)	−0.004	±0.006	±0.005	±0.001	±0.004
(0.070, 0.100)	0.006	±0.006	±0.001	±0.001	±0.000
(0.100, 0.130)	0.010	±0.010	±0.001	±0.001	±0.001
(0.130, 0.200)	0.021	±0.014	±0.001	±0.001	±0.000

TABLE X. Data table of A_N for negatively charged hadron (h^-) in transversely-polarized $p + $ Au collisions as a function of p_T.

$p_T(\text{GeV}/c)$	A_N	δA_N^{stat}	δA_N^{syst}	$\delta A_N^{\text{method}}$	$\delta A_N^{\text{smear}}$
		Forward ($x_F > 0$)			
(1.50, 2.50)	−0.014	±0.007	±0.008	±0.000	±0.008
(2.50, 3.50)	0.000	±0.013	±0.003	±0.000	±0.003
(3.50, 7.00)	0.012	±0.023	±0.009	±0.005	±0.007

(Table continued)

TABLE X. *(Continued)*

$p_T(\text{GeV}/c)$	A_N	δA_N^{stat}	δA_N^{syst}	$\delta A_N^{\text{method}}$	$\delta A_N^{\text{smear}}$
		Backward ($x_F < 0$)			
(1.50, 2.50)	0.002	±0.006	±0.003	±0.001	±0.002
(2.50, 3.50)	−0.006	±0.013	±0.003	±0.001	±0.003
(3.50, 7.00)	0.003	±0.024	±0.001	±0.000	±0.001

TABLE XI. Data table of A_N for positively charged hadron (h^+) in transversely-polarized $p + $ Au collisions as a function of p_T.

$p_T(\text{GeV}/c)$	A_N	δA_N^{stat}	δA_N^{syst}	$\delta A_N^{\text{method}}$	$\delta A_N^{\text{smear}}$
		Forward ($x_F > 0$)			
(1.50, 2.50)	0.010	±0.005	±0.006	±0.000	±0.006
(2.50, 3.50)	−0.005	±0.008	±0.005	±0.001	±0.005
(3.50, 7.00)	0.020	±0.016	±0.008	±0.001	±0.008
		Backward ($x_F < 0$)			
(1.50, 2.50)	0.005	±0.005	±0.002	±0.000	±0.002
(2.50, 3.50)	−0.001	±0.009	±0.001	±0.001	±0.001
(3.50, 7.00)	−0.016	±0.019	±0.006	±0.001	±0.006

TABLE XII. Data table of A_N for negatively charged hadron (h^-) in transversely-polarized $p + $ Au collisions as a function of x_F.

x_F	A_N	δA_N^{stat}	δA_N^{syst}	$\delta A_N^{\text{method}}$	$\delta A_N^{\text{smear}}$
(−0.200, −0.130)	−0.013	±0.027	±0.007	±0.000	±0.007
(−0.130, −0.100)	0.012	±0.018	±0.003	±0.000	±0.003
(−0.100, −0.070)	0.001	±0.009	±0.001	±0.000	±0.001
(−0.070, −0.050)	−0.007	±0.006	±0.004	±0.001	±0.003
(−0.050, −0.040)	−0.002	±0.009	±0.001	±0.000	±0.001
(0.040, 0.050)	−0.018	±0.018	±0.009	±0.001	±0.009
(0.050, 0.070)	−0.007	±0.008	±0.002	±0.001	±0.002
(0.070, 0.100)	−0.002	±0.007	±0.000	±0.000	±0.000
(0.100, 0.130)	−0.001	±0.011	±0.001	±0.000	±0.000
(0.130, 0.200)	−0.005	±0.015	±0.002	±0.002	±0.000

TABLE XIII. Data table of A_N for positively charged hadron (h^+) in transversely-polarized $p + $ Au collisions as a function of x_F.

x_F	A_N	δA_N^{stat}	δA_N^{syst}	$\delta A_N^{\text{method}}$	$\delta A_N^{\text{smear}}$
(−0.200, −0.130)	−0.010	±0.020	±0.003	±0.000	±0.003
(−0.130, −0.100)	0.016	±0.013	±0.004	±0.000	±0.004
(−0.100, −0.070)	0.008	±0.006	±0.001	±0.000	±0.001
(−0.070, −0.050)	−0.004	±0.005	±0.002	±0.000	±0.002
(−0.050, −0.040)	0.000	±0.007	±0.001	±0.000	±0.001
(0.040, 0.050)	0.009	±0.012	±0.005	±0.000	±0.004
(0.050, 0.070)	−0.002	±0.005	±0.002	±0.000	±0.002
(0.070, 0.100)	0.007	±0.004	±0.002	±0.000	±0.002
(0.100, 0.130)	−0.008	±0.008	±0.004	±0.001	±0.004
(0.130, 0.200)	0.017	±0.010	±0.004	±0.001	±0.004

[1] R. D. Klem, J. E. Bowers, H. W. Courant, H. Kagan, M. L. Marshak, E. A. Peterson, K. Ruddick, W. H. Dragoset, and J. B. Roberts, Measurement of asymmetries of inclusive pion production in proton proton interactions at 6 GeV/c and 11.8 GeV/c, Phys. Rev. Lett. **36,** 929 (1976).

[2] J. Antille, L. Dick, L. Madansky, D. Perret-Gallix, M. Werlen, A. Gonidec, K. Kuroda, and P. Kyberd, Spin dependence of the inclusive reaction pp (polarized) $\rightarrow$ $\pi^0 X$ at 24 GeV/c for high p_T π^0 produced in the central region, Phys. Lett. **94B,** 523 (1980).

[3] D. L. Adams *et al.* (FNAL-E704 Collaboration), Analyzing power in inclusive π^+ and π^- production at high x_F with a 200 GeV polarized proton beam, Phys. Lett. B **264,** 462 (1991).

[4] D. L. Adams *et al.* (E581 and E704 Collaboration), Comparison of spin asymmetries and cross-sections in π^0 production by 200 GeV polarized antiprotons and protons, Phys. Lett. B **261,** 201 (1991).

[5] C. E. Allgower, K. W. Krueger, T. E. Kasprzyk, H. M. Spinka, D. G. Underwood, A. Yokosawa *et al.*, Measurement of analyzing powers of π^+ and π^- produced on a hydrogen and a carbon target with a 22-GeV/c incident polarized proton beam, Phys. Rev. D **65,** 092008 (2002).

[6] J. Adams *et al.* (STAR Collaboration), Cross-sections and transverse single-spin asymmetries in forward neutral pion production from proton collisions at $\sqrt{s} = 200$ GeV, Phys. Rev. Lett. **92,** 171801 (2004).

[7] J. H. Lee and F. Videbaek (BRAHMS Collaboration), Single-spin asymmetries of identified hadrons in polarized p + p at $\sqrt{s} = 62.4$ and 200 GeV, AIP Conf. Proc. **915,** 533 (2007).

[8] B. I. Abelev *et al.* (STAR Collaboration), Forward neutral pion transverse single-spin asymmetries in p + p collisions at $\sqrt{s} = 200$ GeV, Phys. Rev. Lett. **101,** 222001 (2008).

[9] I. Arsene *et al.* (BRAHMS Collaboration), Single transverse spin asymmetries of identified charged hadrons in polarized pp collisions at $\sqrt{s} = 62.4$ GeV, Phys. Rev. Lett. **101,** 042001 (2008).

[10] L. Adamczyk *et al.* (STAR Collaboration), Transverse single-spin asymmetry and cross-section for π^0 and η mesons at large Feynman-x in polarized $p + p$ collisions at $\sqrt{s} = 200$ GeV, Phys. Rev. D **86,** 051101 (2012).

[11] A. Adare *et al.* (PHENIX Collaboration), Measurement of transverse-single-spin asymmetries for midrapidity and forward-rapidity production of hadrons in polarized p + p collisions at $\sqrt{s} = 200$ and 62.4 GeV, Phys. Rev. D **90,** 012006 (2014).

[12] A. Adare *et al.* (PHENIX Collaboration), Cross section and transverse single-spin asymmetry of η mesons in $p^\uparrow + p$ collisions at $\sqrt{s} = 200$ GeV at forward rapidity, Phys. Rev. D **90,** 072008 (2014).

[13] J. Adam *et al.* (STAR Collaboration), Measurement of transverse single-spin asymmetries of π^0 and electromagnetic jets at forward rapidity in 200 and 500 GeV transversely polarized proton-proton collisions, Phys. Rev. D **103,** 092009 (2021).

[14] D. W. Sivers, Single-spin production asymmetries from the hard scattering of point-like constituents, Phys. Rev. D **41,** 83 (1990).

[15] D. W. Sivers, Hard scattering scaling laws for single-spin production asymmetries, Phys. Rev. D **43,** 261 (1991).

[16] J. C. Collins, Fragmentation of transversely polarized quarks probed in transverse momentum distributions, Nucl. Phys. **B396,** 161 (1993).

[17] J. Qiu and G. F. Sterman, Single transverse spin asymmetries in hadronic pion production, Phys. Rev. D **59,** 014004 (1998).

[18] C. Kouvaris, J. W. Qiu, W. Vogelsang, and F. Yuan, Single transverse-spin asymmetry in high transverse momentum pion production in pp collisions, Phys. Rev. D **74,** 114013 (2006).

[19] Y. Koike and K. Tanaka, Universal structure of twist-3 soft-gluon-pole cross-sections for single transverse-spin asymmetry, Phys. Rev. D **76,** 011502(R) (2007).

[20] Y. Koike and T. Tomita, Soft-fermion-pole contribution to single-spin asymmetry for pion production in pp collisions, Phys. Lett. B **675,** 181 (2009).

[21] K. Kanazawa and Y. Koike, New analysis of the single transverse-spin asymmetry for hadron production at RHIC, Phys. Rev. D **82,** 034009 (2010).

[22] Z. B. Kang, J. W. Qiu, W. Vogelsang, and F. Yuan, An observation concerning the process dependence of the sivers functions, Phys. Rev. D **83,** 094001 (2011).

[23] K. Kanazawa and Y. Koike, A phenomenological study on single transverse-spin asymmetry for inclusive light-hadron productions at RHIC, Phys. Rev. D **83,** 114024 (2011).

[24] Z. B. Kang and A. Prokudin, Global fitting of single-spin asymmetry: An attempt, Phys. Rev. D **85,** 074008 (2012).

[25] H. Beppu, K. Kanazawa, Y. Koike, and S. Yoshida, Three-gluon contribution to the single-spin asymmetry for light hadron production in pp collision, Phys. Rev. D **89,** 034029 (2014).

[26] A. Metz and D. Pitonyak, Fragmentation contribution to the transverse single-spin asymmetry in proton-proton collisions, Phys. Lett. B **723,** 365 (2013); **762,** 549(E) (2016).

[27] K. Kanazawa, Y. Koike, A. Metz, and D. Pitonyak, Towards an explanation of transverse single-spin asymmetries in proton-proton collisions: The role of fragmentation in collinear factorization, Phys. Rev. D **89,** 111501(R) (2014).

[28] L. Gamberg, Z. Kang, D. Pitonyak, and A. Prokudin, Phenomenological constraints on A_N in $p^\uparrow p \rightarrow \pi X$ from Lorentz invariance relations, Phys. Lett. B **770,** 242 (2017).

[29] J. Cammarota, L. Gamberg, Z. B. Kang, J. A. Miller, D. Pitonyak, A. Prokudin, T. C. Rogers, and N. Sato (Jefferson Lab Angular Momentum Collaboration), Origin of single transverse-spin asymmetries in high-energy collisions, Phys. Rev. D **102,** 054002 (2020).

[30] F. Gelis, E. Iancu, J. Jalilian-Marian, and R. Venugopalan, The color glass condensate, Annu. Rev. Nucl. Part. Sci. **60,** 463 (2010).

[31] Z. B. Kang and F. Yuan, Single-spin asymmetry scaling in the forward rapidity region at RHIC, Phys. Rev. D **84,** 034019 (2011).

[32] Y. V. Kovchegov and M. D. Sievert, A new mechanism for generating a single transverse spin asymmetry, Phys. Rev. D **86,** 034028 (2012); **86,** 079906(E) (2012).

[33] A. Schäfer and J. Zhou, Transverse single-spin asymmetry in direct photon production in polarized pA collisions, Phys. Rev. D **90,** 034016 (2014).

[34] J. Zhou, Transverse single-spin asymmetry in Drell-Yan production in polarized pA collisions, Phys. Rev. D **92,** 014034 (2015).

[35] Y. Hatta, B. W. Xiao, S. Yoshida, and F. Yuan, Single-spin asymmetry in forward *pA* collisions, Phys. Rev. D **94,** 054013 (2016).

[36] Y. Hatta, B. W. Xiao, S. Yoshida, and F. Yuan, Single-spin asymmetry in forward *pA* collisions II: Fragmentation contribution, Phys. Rev. D **95,** 014008 (2017).

[37] C. Aidala *et al.* (PHENIX Collaboration), Nuclear dependence of the transverse single-spin asymmetry in the production of charged hadrons at forward rapidity in polarized $p + p$, $p + \mathrm{Al}$, and $p + \mathrm{Au}$ collisions at $\sqrt{s_{NN}} = 200$ GeV, Phys. Rev. Lett. **123,** 122001 (2019).

[38] J. Adam *et al.* (STAR Collaboration), Comparison of transverse single-spin asymmetries for forward π^0 production in polarized pp, $p\mathrm{Al}$ and $p\mathrm{Au}$ collisions at nucleon pair c.m. energy $\sqrt{s_{\mathrm{NN}}} = 200$ GeV, Phys. Rev. D **103,** 072005 (2021).

[39] K. Adcox *et al.* (PHENIX Collaboration), PHENIX detector overview, Nucl. Instrum. Methods Phys. Res., Sect. A **499,** 469 (2003).

[40] H. Akikawa *et al.* (PHENIX Collaboration), PHENIX muon arms, Nucl. Instrum. Methods Phys. Res., Sect. A **499,** 537 (2003).

[41] A. Adare *et al.* (PHENIX Collaboration), Nuclear-modification factor for open-heavy-flavor production at forward rapidity in $\mathrm{Cu} + \mathrm{Cu}$ collisions at $\sqrt{s_{NN}} = 200$ GeV, Phys. Rev. C **86,** 024909 (2012).

[42] M. Allen *et al.* (PHENIX Collaboration), PHENIX inner detectors, Nucl. Instrum. Methods Phys. Res., Sect. A **499,** 549 (2003).

[43] S. Adachi *et al.*, Trigger electronics upgrade of PHENIX muon tracker, Nucl. Instrum. Methods Phys. Res., Sect. A **703,** 114 (2013).

[44] RHIC Polarimetry Group, RHIC polarization for Runs 9–12, RHIC/CAD Accelerator Physics Note 490, 2018.

[45] C. Aidala *et al.* (PHENIX Collaboration), Nuclear-modification factor of charged hadrons at forward and backward rapidity in $p + \mathrm{Al}$ and $p + \mathrm{Au}$ collisions at $\sqrt{s_{NN}} = 200$ GeV, Phys. Rev. C **101,** 034910 (2020).

[46] A. Adare *et al.* (PHENIX Collaboration), Cold-nuclear-matter effects on heavy-quark production at forward and backward rapidity in $\mathrm{d} + \mathrm{Au}$ collisions at $\sqrt{s_{NN}} = 200$ GeV, Phys. Rev. Lett. **112,** 252301 (2014).

[47] T. Sjostrand, S. Mrenna, and P. Z. Skands, PYTHIA6.4 Physics and Manual, J. High Energy Phys. 05 (2006) 026.

[48] M. Gyulassy and X. Wang, HIJING1.0: A Monte Carlo program for parton and particle production in high-energy hadronic and nuclear collisions, Comput. Phys. Commun. **83,** 307 (1994).

[49] A. Adare *et al.* (PHENIX Collaboration), Identified charged hadron production in $p + p$ collisions at $\sqrt{s} = 200$ and 62.4 GeV, Phys. Rev. C **83,** 064903 (2011).

[50] G. Agakishiev *et al.* (STAR Collaboration), Identified hadron compositions in $p + p$ and $\mathrm{Au} + \mathrm{Au}$ collisions at high transverse momenta at $\sqrt{s_{NN}} = 200$ GeV, Phys. Rev. Lett. **108,** 072302 (2012).

[51] A. Adare *et al.* (PHENIX Collaboration), Spectra and ratios of identified particles in $\mathrm{Au} + \mathrm{Au}$ and $d + \mathrm{Au}$ collisions at $\sqrt{s_{NN}} = 200$ GeV, Phys. Rev. C **88,** 024906 (2013).

[52] S. Agostinelli *et al.* (GEANT4 Collaboration), GEANT4–a simulation toolkit, Nucl. Instrum. Methods Phys. Res., Sect. A **506,** 250 (2003).

[53] R. L. Workman *et al.* (Particle Data Group), Review of particle physics, Prog. Theor. Exp. Phys. **2022,** 083C01 (2022).

[54] J. Allison *et al.*, Recent developments in GEANT4, Nucl. Instrum. Methods Phys. Res., Sect. A **835,** 186 (2016).

[55] C. Aidala *et al.* (PHENIX Collaboration), Cross section and transverse single-spin asymmetry of muons from open heavy-flavor decays in polarized $p + p$ collisions at $\sqrt{s} = 200$ GeV, Phys. Rev. D **95,** 112001 (2017).

[56] C. Aidala *et al.* (PHENIX Collaboration), Single-spin asymmetry of J/ψ production in $p + p$, $p + \mathrm{Al}$, and $p + \mathrm{Au}$ collisions with transversely polarized proton beams at $\sqrt{s_{NN}} = 200$ GeV, Phys. Rev. D **98,** 012006 (2018).

[57] G. G. Ohlsen and P. W. Keaton, Techniques for measurement of spin-1/2 and spin-1 polarization analyzing tensors, Nucl. Instrum. Methods Phys. Res., Sect. A **109,** 41 (1973).

[58] J. Zhou, Single-spin asymmetries in forward p-p/A collisions revisited: The role of color entanglement, Phys. Rev. D **96,** 034027 (2017).

[59] S. Benić and Y. Hatta, Single-spin asymmetry in forward *pA* collisions: Phenomenology at RHIC, Phys. Rev. D **99,** 094012 (2019).

[60] Y. V. Kovchegov and M. G. Santiago, Lensing mechanism meets small-*x* physics: Single transverse spin asymmetry in $p^{\uparrow} + p$ and $p^{\uparrow} + A$ collisions, Phys. Rev. D **102,** 014022 (2020).